PAPER

Nitrogen-doped Fe₃C@C particles as an efficient heterogeneous photo-assisted Fenton catalyst†

Xiaoling Yang,‡[a] Chengjia Li,‡[a] Jianfei Huang,[b] Yanyan Liu,[a] Wei Chen,[a] Jianhua Shen,[a] Yihua Zhu*[a] and Chunzhong Li[a]

Designing high-efficiency heterogeneous photo-assisted Fenton catalysts is the key to harnessing solar energy for promoting the Fenton process in water treatment. Herein we developed nitrogen-doped Fe₃C@C particles by thermally treating Fe₃O₄ precursor with dicyandiamide. The as-prepared Fe–N–C hybrid material was comprehensively characterized by electron microscopy, various spectroscopic techniques and so forth to confirm the compositions and structures. The band gap of nitrogen-doped Fe₃C@C particles was about 1.6 eV. Methylene blue was used as a model organic contaminant to test the photo-assisted Fenton activity of the nitrogen-doped Fe₃C@C particles, with optimal dosages of H₂O₂ and the catalyst itself, which showed excellent efficiency in removing the model contaminant, demonstrating that the as-prepared hybrids can work as a highly efficient photo-assisted Fenton catalyst.

Introduction

The pollution from the wastewater in dye-involved industry has become a serious threat to the environment and society because of the toxicity and non-biodegradability of various organic dyes.[1,2] Therefore, considerable research work has been focused on removing organic contaminants from wastewater. Industrially realized methods including absorption, flocculation and chemical oxidation have been applied to address this problem.[3–5] Among chemical oxidation technologies that lead to complete destruction of organic pollutant molecules, the Fenton reaction, where ferrous ions and hydrogen peroxide react to generate highly reactive hydroxyl radicals in aqueous solution, has drawn intensive attention owing to its reliable performance. In conventional homogeneous Fenton systems composed of dissolved Fe^{2+}/Fe^{3+} species and hydrogen peroxide, hydroxyl radicals generated within the system can rapidly oxidize organic pollutants.[6–8] Compared with other methods, the Fenton process is environmentally friendly, cost-effective, and simple to operate.[9] However, there are some drawbacks associated with homogeneous Fenton systems, including acidic nature of the system (pH 2.5–4), by-products of iron sludge and difficult recovery.[10,11]

Heterogeneous Fenton-like catalysts, which employ various active iron-containing solid-state components to sustain the Fenton reaction, represent a promising alternative for overcoming the as-mentioned problems associated with homogeneous catalysts.[12] Considering the introduction of solar energy and photocatalysis promoting the catalytic reaction,[13,14] in further attempts to facilitate the process, the technology that combines illumination and Fenton reaction, known as photo-assisted Fenton process, is becoming an appealing strategy due to the accelerated Fenton process as a result of the light-promoted production of hydroxyl radicals.[15–17] Two main types of heterogeneous photo-Fenton catalyst systems are being developed. One is supported catalysts such as iron or iron oxide nanoparticles combined with SBA-15, zeolite, clay or montmorillonite,[18–21] and the other is single-substance materials such as metallic oxides, spinel ferrites (MFe₂O₄) with different cations (M = Cu, Zn, Ni and Co).[22–24] The structure of the materials in the former type of catalysts is that Fenton-active iron or iron compounds dispersed onto solid-state supports, while the latter type of catalysts employ various forms of iron compounds directly as Fenton catalysts without Fenton-inactive supporting materials. This not only avoids the cost of supported materials, but also gets rid of complicated synthetic procedures in production of the catalysts. In addition, the inherent magnetic behavior can overcome the drawback of difficulty separation. On account of these factors, in this investigation we seek to magnetic support-free catalysts with high catalytic activity and light responsiveness for photo-assisted Fenton process.

Iron carbide (Fe₃C) has attracted significant interests in lithium ion storage, bioelectricity, microwave absorbents, detection of hydrogen peroxide, and fuel cells due to its outstanding magnetic property, thermal stability, high oxidation resistance, mechanical strength, and catalytic activity.[25–31] Despite the existing investigations on the functionality of Fe₃C/

[a]Key Laboratory for Ultrafine Materials of Ministry of Education, School of Materials Science and Engineering, East China University of Science and Technology, Shanghai 200237, China. E-mail: yhzhu@ecust.edu.cn

[b]Department of Chemistry and Biochemistry, University of California, Santa Barbara, Santa Barbara 93106, CA, USA

‡ These authors contributed equally to this work.

carbon materials in electrochemical applications, rarely have there been reports demonstrating Fe–N–C materials as an efficient platform of photo-assisted Fenton-reaction catalyst. It is found that a mixture of reactants containing iron and carbon sources is likely to produce nitrogen-doped graphitic carbon layer wrapping Fe_3C nanostructures after appropriate thermal annealing, which provides a simple route toward nitrogen-doped Fe_3C@C particles.[31,32] Combining the fact that photo-catalytically active phase of C_3N_4 can be generated under thermal annealing with C- and N-containing carbon sources in presence,[33] we herein propose a designed protocol to attain graphitic structure-present Fe–N–C hybrid. In this work, we synthesized light-responding nitrogen-doped Fe_3C@C particles (NFC) as an efficient heterogeneous photo-assisted Fenton catalyst for degradation of organic pollutants. The molecular carbon–nitrogen fragments released from pyrolysis of dicyandiamide replaced oxygen species in the Fe_3O_4 precursor, leading to reduced iron and incorporation of carbon into the iron phase to give Fe_3C. The thin layers of nitrogen-doped graphite structure on the surface of the hybrid not only offered enhanced adsorption of pollutant molecules but may contribute to boosting the Fenton process with its responsiveness to light irradiation.

In this work, we synthesized light-responding nitrogen-doped Fe_3C@C particles (NFC) as an efficient heterogeneous photo-assisted Fenton catalyst for degradation of organic pollutants. The molecular carbon–nitrogen fragments released from pyrolysis of dicyandiamide replaced oxygen species in the Fe_3O_4 precursor, leading to reduced iron and incorporation of carbon into the iron phase to give Fe_3C. The thin layers of nitrogen-doped graphite structure on the surface of the hybrid not only offered enhanced adsorption of pollutant molecules but may contribute to boosting the Fenton process with its responsiveness to light irradiation. In this work, a series of nitrogen-doped Fe_3C@C particles with the amount of dicyandiamide was 0.2, 0.5, 0.8, and 1.2 g were prepared and were denoted as NFC-2, NFC-5, NFC-8, NFC-12, respectively. The catalytic activity of NFC was investigated with methylene blue (MB) as model pollutant in photo-assisted Fenton reaction tested in neutral pH. The effect of dosage of the catalyst and H_2O_2 on degradation of MB were investigated. As a result, nitrogen-doped Fe_3C@C particles exhibited excellent catalytic ability with the removal rates of methylene blue achieving 82% in 10 minutes and 95% in 20 minutes under the optimal condition.

Experimental

Material and reagents

All the reagents were purchased from Shanghai Chemical Reagent Co. All chemicals were analytical grade and used without further purification. Deionized water was used for all experiments.

Preparation of Fe_3O_4

2.16 g $FeCl_3 \cdot 6H_2O$, 0.5 g trisodium citrate and 2.0 g NaAc were dissolved in 40 mL ethylene glycol and were subject to magnetic stirring for 30 minutes. Then, the obtained yellow solution was transformed into a 100 mL Teflon-lined stainless-steel autoclave, and heated at 200 °C for 10 h. After the autoclave cooled to room temperature, the obtained black products were washed with ethanol and deionized water for three times, respectively, and then left to dry at 60 °C for about 6 h.

Preparation of nitrogen-doped Fe_3C@C particles

0.5 g of the obtained Fe_3O_4 particles were dispersed in 100 mL ethanol by ultrasonication for 10 minutes. Then, a cleaned nickel foam substrate was immersed into the suspension. After the ethanol evaporated away, the nickel foam substrate was dried at 60 °C for 4 h. Subsequently, a varied amount (0.2, 0.5, 0.8 and 1.2 g) of dicyandiamide was put into an alumina crucible and the dried nickel foam substrate was placed over the alumina crucible. The alumina crucible with the nickel foam on it was transferred to a tube furnace and heated to 550 °C for 2 h at a ramp rate of 5 °C min^{-1} under nitrogen atmosphere. After being cooled to room temperature, the obtained dark products were peeled off from the nickel foam by ultrasonication in ethanol, collected by a neodymium magnet and left to dry up at 60 °C for 4 h.

Photo-assisted Fenton degradation of methylene blue

The catalytic activity of NFC as heterogeneous photo-Fenton catalysts was investigated by degrading methylene blue as the model organic pollutant. A Xenon lamp (Solar-500) equipped with a solar spectrum simulation filter (AM 1.5) was used as the light source. All degradation reactions were conducted in a 150 mL flask with constant mechanical stirring at room temperature. The irradiation intensity was 70 mW cm^{-2} (calibrated by FZ-400 optical power meter) at the center position of flask. A certain amount of NFC catalysts were added into 80 mL aqueous solution containing 10 mg L^{-1} MB. Before irradiation, the suspension was stirred for 30 min in dark to reach adsorption–desorption equilibrium of methylene blue molecules on the catalysts' surface, so that the following decrease in the concentration of MB can be fairly attributed to the photo-assisted Fenton process. Upon initiation of the photo-assisted Fenton reactions, irradiation was provided with instant addition of a certain amount of H_2O_2 to the mixed solution. During the test, about 4 mL mixed solution was withdrawn from the system at given intervals. The concentration of MB in the sample was determined by recording the absorbance of the supernatant at the wavelength of 664 nm by UV-vis spectroscopy.

Characterization

Scanning electron microscopy (SEM) and transmission electron microscopy (TEM) were used to examine the morphologies and microstructures of all samples, operated on an S-4800 field-emission scanning electron microscope equipped with an energy dispersive X-ray analyzer (EDX) and a JEM-2100 transmission electron microscope, respectively. Powder X-ray diffraction (XRD) measurements were performed on an X-ray diffractometer (RIGAKU, D/MAX 2550VB/PC, Japan) with Cu Kα radiation to verify the crystalline structure of the catalysts.

The UV-vis spectra were recorded on a UV-vis spectrometer (UNICO UV-2102PC) at room temperature. The magnetization curves of the products were measured with a vibrating sample magnetometer (LAKE SHORE, 7407). X-ray photoelectron spectroscopy (XPS) spectra were obtained with a magnesium anode, which were used to characterize the types of carbon, nitrogen and metal elements. All XPS data were calibrated using the C 1s peak at 284.8 eV as an internal standard.

Results and discussion

The preparation procedures of NFC for ultrafast oxidative decomposition of MB are illustrated in Fig. 1. First, the Fe_3O_4 particles were prepared according to our previous work.[34] After the magnetic Fe_3O_4 particles in the suspension solution were loaded on a nickel foam substrate by solvent evaporation, they were subject to 550 °C thermal annealing and reacted with dicyandiamide under nitrogen atmosphere to form NFC hybrids. After cooled to room temperature, the final products were peeled off from nickel foam substrate by ultrasonication in ethanol.

Morphology and structure

The morphologies and structures of NFC and the Fe_3O_4 precursor were characterized by SEM and TEM. As shown in Fig. 2a and b, the as-prepared Fe_3O_4 particles are well distributed with a diameter of about 250 nm. Their surfaces are rough, which is consistent with the fact that an individual Fe_3O_4 particle is composed of many smaller Fe_3O_4 particles.[35] As displayed in Fig. 2c and d, after the Fe_3O_4 particles were converted to nitrogen-doped $Fe_3C@C$ particles, the latter were found to be partly connected to one another due to the existence of the carbon outer layers generated in the annealing process.[36]

To gain more structural information of the as-prepared hybrid particles, TEM was employed. As can be seen in Fig. 3a, the hybrid particles have outer carbon shells which are about 10 nm in thickness. As displayed in Fig. 3b, the lattice distance of the outer shell of the hybrid particle is found to be 0.34 nm, which corresponds to the (002) plane of graphite, respectively.[37] As shown in Fig. 3c, the lattice distance of the inner core of the hybrid particle is found to be 0.209 nm, which corresponds well to the (111) plane in Fe_3C, confirming the presence of Fe_3C core.

The crystalline structures of the products with different Fe_3O_4-to-dicyandiamide ratios were characterized by powder X-

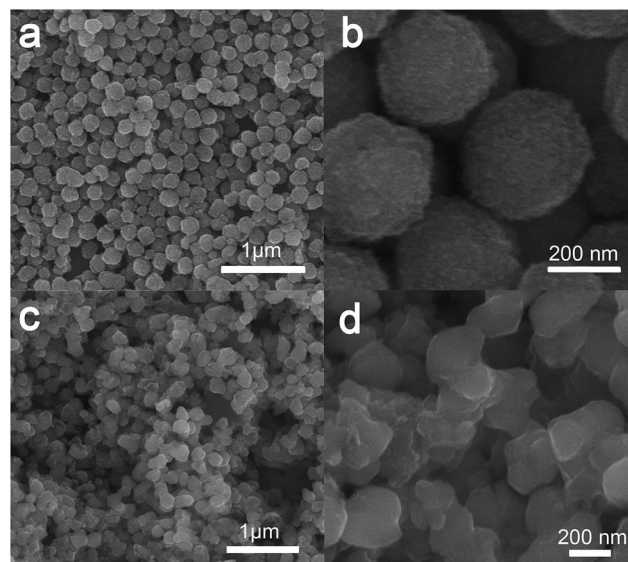**Fig. 2** SEM images of the as-prepared (a, b) Fe_3O_4 nanoparticles and (c, d) the nitrogen-doped $Fe_3C@C$ particles.

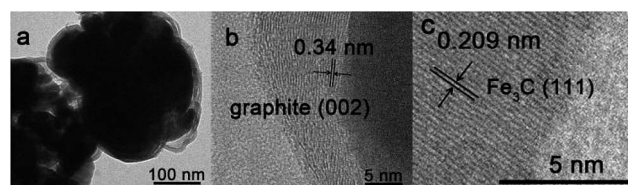**Fig. 3** (a) TEM image and (b, c) HRTEM images of the nitrogen-doped $Fe_3C@C$ particles.

ray diffraction (XRD). As seen in Fig. 4a, in NFC-2, the diffraction peaks at $2\theta = 41.2°$ and 47.9° are in agreement with the characteristic peaks of Fe_4N (JCPDS no. 83-0875), while the peaks at 37.7°, 43.7° 44.9° and 45.9° can be ascribed to Fe_3C (JCPDS no. 72-1110). In NFC-5, the diffraction peaks at 37.7°, 41.5° and 43.2° can be attributed to Fe_3C (JCPDS no. 89-2005), and the peaks of Fe_5C_2 also appeared at 44.1° and 44.9° (JCPDS no. 51-0997). In NFC-8, the diffraction peaks can be ascribed to Fe_3C, Fe_2N and Fe_5C_2 with their peaks identified at 37.7°, 43.2°, 76.8° for Fe_3C (JCPDS no. 89-2005), at 42.9°, 56.7°, 67.7° for Fe_2N (JCPDS no. 72-2126), and peaks at 44.1°, 44.9° for Fe_5C_2 (JCPDS no. 51-0997). In NFC-12, the diffraction peaks at 44.6°, 51.5° can be ascribed to Fe_5C_2 (JCPDS no. 51-0997) and the peaks at 41.5° and 43.2° can be ascribed to Fe_3C (JCPDS no. 89-2005). Accordingly, as shown in the patterns, when the amount of dicyandiamide varies from 0.2 g to 0.5 g, the main products are Fe_4N and Fe_3C. With the amount of dicyandiamide increasing, the peaks of Fe_4N disappear and the peaks of Fe_3C become stronger and sharper in NFC-5 and NFC-8, which indicates that the phase of Fe_3C becomes the major component in the resulted products. For NFC-12, the intensity of diffraction peaks of Fe_3C and Fe_5C_2 drops. The patterns from NFC-2 to NFC-12 indicate that the hybrids of NFC-5 and NFC-8 have better crystallinity for iron carbides, which are the main components rather than
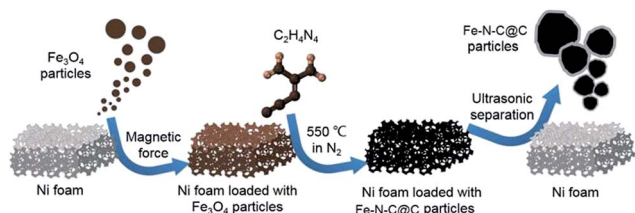

Fig. 1 The preparation process of the nitrogen-doped $Fe_3C@C$ particles (NFC).

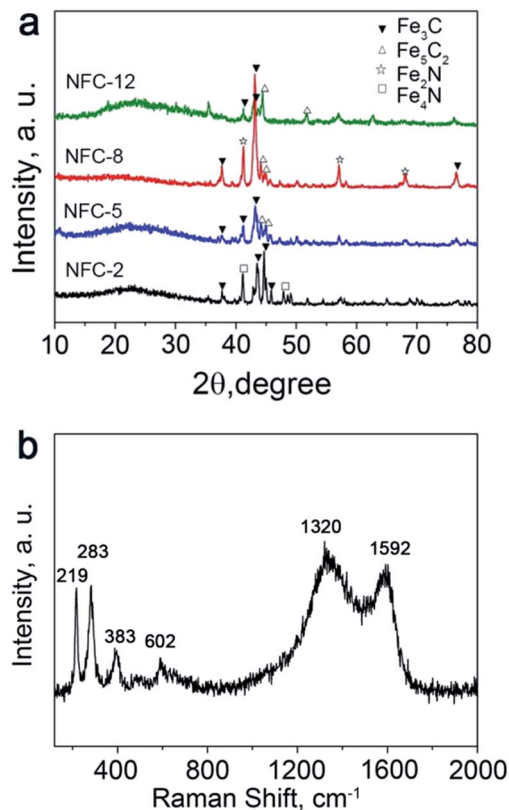Fig. 4 (a) XRD patterns and (b) Raman spectrum of the nitrogen-doped Fe$_3$C@C particles.

Fig. 5 (a) Kubelka–Munk plot for NFC-5 and NFC-8, (b) the MB degradation efficiency of NFC-5 and NFC-8.

being amorphous. Fig. 4b shows the Raman spectrum of NFC-8, the G peak at 1592 cm^{-1} and D peak at 1320 cm^{-1} correspond to the carbon with both graphitic and amorphous structures.[38] The peaks at lower Raman shift of 219, 283, 383, and 602 cm^{-1} suggest presence of the by-product C$_3$N$_4$,[39] which derived from the polycondensation of C–N gas released from the dicyandiamide during the annealing process.

Fig. 5a and b show Kubelka–Munk plot and the MB degradation efficiency of NFC-5 and NFC-8, respectively. The Fig. S1† shows the UV-visible absorption ability of NFC-8 is superior to NFC-5. As shown in Fig. 5a, the Kubelka–Munk plot shows the band gap from 1.65 eV for NFC-5 to 1.64 eV for NFC-8, it indicates that the as-prepared Fe–N–C hybrid material can absorption visible light effectively, which may contribute to better utilization efficiency of irradiation in a photo-assisted Fenton process. Consistently, in Fig. 5b, it is found that the degradation efficiency of NFC-8 is higher compared to NFC-5. Considering the crystallinity as well as the degradation efficiency, NFC-8 was selected as the heterogeneous photo-assisted Fenton catalyst to be further studied.

The X-ray photoelectron spectroscopy (XPS) of NFC-8 as shown in Fig. 6 was obtained to analyze the surface state of the nitrogen-doped Fe$_3$C@C particles. The XPS survey scan of the NFC-8 in Fig. S2† and mapping of Fig. S3† show the existence of elements of C, N, Fe, and O in the hybrid particles. The spectrum indicates that the content of carbon is much higher than other elements, corresponding to the carbon layers on the
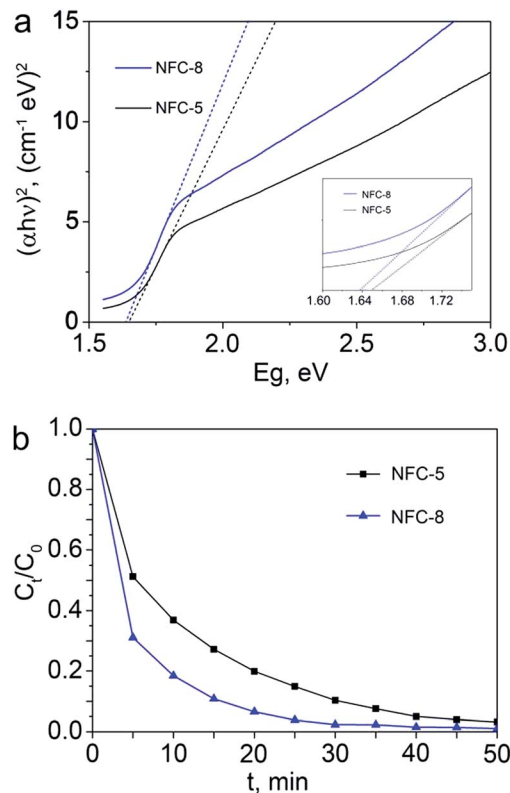
surface of nitrogen-doped Fe$_3$C@C particles. In Fig. 6a, with the decoupled C 1s peaks at 284.8 eV and 286.4 eV we can confirm the presence of nitrogen-doped graphitic structure.[40,41]

The N 1s spectrum in Fig. 6b shows two deconvoluted peaks at binding energies of 398.5 and 400.5 eV, corresponding to the sp^2-hybridized nitrogen C=N–C involved in the triazine rings
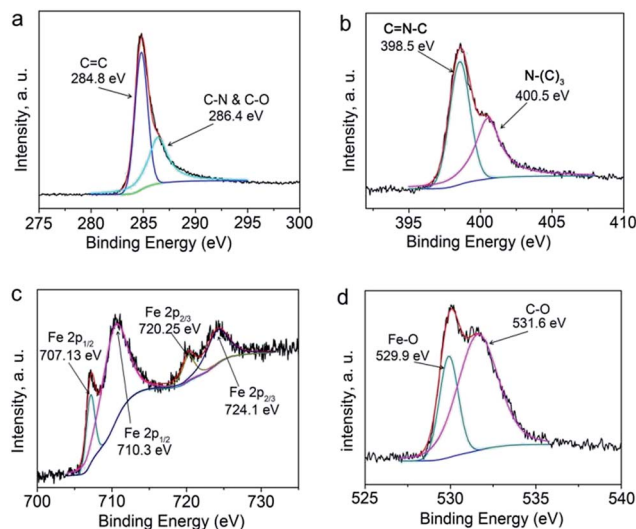

Fig. 6 XPS spectra of nitrogen-doped Fe$_3$C@C particles: (a) C 1s, (b) N 1s, (c) Fe 2p, (d) O 1s.

and the bridged nitrogen atoms N–(C)$_3$, respectively,[42] further confirming the carbon outer shells of nitrogen-doped graphitic nature.[43] As shown in Fig. 6c, the spectrum of Fe 2p can be deconvoluted into four peaks at 707.13, 710.3, 720.25 and 724.1 eV, respectively. The peaks at 707.13 and 720.25 eV can be ascribed to the Fe 2p$_{1/2}$ and Fe 2p$_{3/2}$ for Fe, and the peaks at 710.3 eV and 724.1 eV are ascribed to the Fe 2p$_{1/2}$ and Fe 2p$_{3/2}$ for Fe^{3+}.[44] In Fig. 6d, the two deconvoluted peaks at 529.9 and 531.6 eV can be attributed to absorbed oxygen and Fe–O bonds, respectively. The latter may from residual iron oxide. In sum, the patterns of Fig. 6(a–d) indicate that the outer shells of the hybrid particles are composed of nitrogen-doped graphitic carbon.

The magnetic properties of the NFC-8 and the Fe$_3$O$_4$ precursor were compared. As seen in Fig. 7a, despite containing a portion of non-magnetic contents of carbon shells, the NFC-8 still demonstrates a saturation magnetization (M_s) value of 100.91 emu g^{-1}, while the M_s of the purely magnetic Fe$_3$O$_4$ precursor is only 43.52 emu g^{-1}. This is due to the existence of the ferromagnetic Fe$_3$C, whose reported M_s value reaches as high as 140 emu g^{-1}.[45] The magnetization curve for NFC-8 features an obvious magnetic hysteresis loop, indicating the NFC-8 to be a ferromagnetic material. As seen in Fig. 7b, the magnetic separation of NFC-8 particles in the methylene blue solution is compared with pure methylene blue solution. This shows the excellent magnetic properties of NFC-8 particles can be facilely recollected from the solution by a magnet. Such

excellent magnetically separable property is desirable for facilitating reuse of the catalysts, which may shorten the cycle duration of overall water treatment in practical applications. The Fig. S4† shows recycling performance of NFC-8, it demonstrates the stable catalytic activities of nitrogen-doped Fe$_3$C@C particles.

Catalytic activities of NFC-8 in photo-assisted Fenton process

The catalytic activities of NFC-8 for degradation of organic pollutants were evaluated with the methylene blue (MB) as model pollutant. The initial concentration of MB was 10 mg L^{-1} and NFC-8 particles were dispersed in MB solution under stirring in dark for 30 minutes to achieve absorption–desorption equilibrium before commencement of Fenton-based degradation reaction. Then, the concentrations of MB as detected after absorption–desorption equilibrium were referred as C_0. The catalytic degradation commenced upon introducing illumination as well as H$_2$O$_2$ to the system, and the concentration of MB was recorded using a small amount of sample taken from the MB solution at intervals.

First, the effect of the dosage of catalysts on the degradation efficiency was probed. As illustrated in Fig. 8a, the maximum degradation efficiency takes place with the dosage of the catalysts as 0.75 g L^{-1}. The removal efficiency is 82% at a runtime of 10 minutes and 95% at 20 minutes, respectively. The degradation activities increased with the amount of the catalysts increasing from 0.25 g L^{-1} to 0.75 g L^{-1}, but showed no
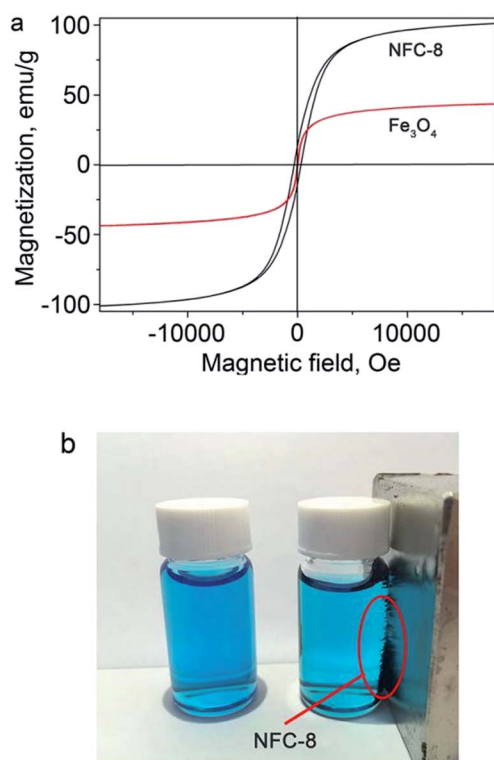

Fig. 7 (a) Magnetic hysteresis loops of NFC-8 and Fe$_3$O$_4$ at room temperature, (b) digital photograph of NFC-8 immobilized by a magnet.
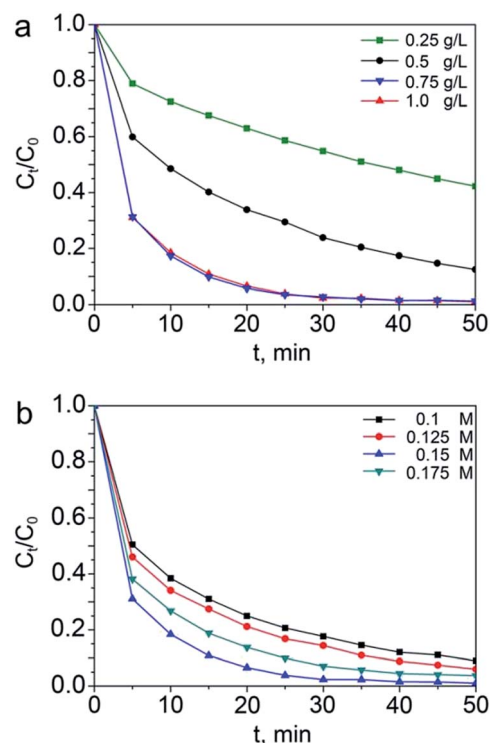

Fig. 8 NFC-8 particles as heterogeneous photo-Fenton catalysts for the degradation of MB under neutral pH. (a) Effect of NFC-8 dosage on MB degradation (initial concentrate of H$_2$O$_2$: 0.15 M); (b) effect of H$_2$O$_2$ dosage on MB degradation (initial concentrate of catalysts: 0.75 g L^{-1}).

enhancement with higher catalyst dosage. With relatively larger amount of NFC-8, more catalysts in the solution can contribute to the photo-Fenton reaction by efficiently absorbing light and acting as the iron ions source. However, the magnetic particles may have the tendency to aggregate when the concentration reaches a certain value, which makes the actual active surfaces and catalytic active sites decrease.[46,47] To achieve the optimal performance of the catalysts, the effect of amount of H_2O_2 on the degradation activity was also studied with the dosage of catalysts set as 0.75 g L^{-1}. It can be found in Fig. 8b that the removal efficiency increases as the amount of H_2O_2 increases from 0.1 M to 0.15 M, but drops lower when the its amount further increases to 0.175 M. Therefore, the optimal amount of H_2O_2 is confirmed as 0.15 M. The observed phenomenon may be ascribed to that the generation of hydroxyl radicals ($^{\cdot}$OH) which works as the key oxidant in Fenton process is favored when the concentration of H_2O_2 increases, leading to more reactive species to attack and destruct the MB molecules. However, when the amount of H_2O_2 continues to increase, the excessive H_2O_2 would react with the generated hydroxyl radicals ($^{\cdot}$OH) before them can oxidize the organic compounds, contributing to loss of degradation efficiency.[46,48] Herein, to achieve optimal efficiency, the optimal dosage of the catalysts and H_2O_2 are found to be 0.75 g L^{-1} and 0.15 M, respectively.

To confirm that the effective catalytic activities of NFC-8 particles on degradation of MB in a photo-assisted Fenton process synergistically realized by NFC-8 particles and H_2O_2, the control experiments with MB mixed with H_2O_2 or NFC-8 particles alone have been conducted. Fig. 9a shows the degradation efficiency of the NFC-8 alone (red), H_2O_2 alone (black) and the NFC-8 with H_2O_2 (blue). It can be seen that the concentration of MB decreases very slightly with only the NFC-8 or H_2O_2 alone. Therefore, only NFC-8 particles or H_2O_2 cannot quickly degrade the MB. The excellent catalytic activity on degradation of MB can be confirmed to the combined effect from NFC-8 particles and H_2O_2 leading to the Fenton reaction. The comparison of the degradation efficiency between NFC-8 particles and Fe_3O_4 particles is also shown, and the result indicate that NFC-8 particles are more efficient than the Fe_3O_4 precursor for the degradation of MB. This can be an outcome together led to by the additional utilization of light irradiation enabled photoactive C_3N_4 in the hybrid as well as inherent property difference between Fe_3O_4 and Fe_3C. To prove that the Fenton degradation of MB was facilitated irradiation, irradiation-free test was also run with NFC-8, as shown in Fig. 9b. Clearly observed, introducing of irradiation can promote the degradation efficiency of MB.

The degradation efficiency of MB in photo-assisted Fenton process catalyzed by NFC-8 was much fast than previous reported supported catalysts[18–21] and spinel ferrite-based materials,[22–24] mainly due to the unique structure of nitrogen-doped $Fe_3C@C$ particles. A small amount of co-formed C_3N_4 in the graphitic carbon may extends the light absorption of the material, leading to positive utilization of light. Photo-induced electrons can be efficiently transported in the graphitic carbon structure. In the photo-assisted Fenton process, the reaction between ferrous ions and hydrogen peroxide was accelerated by photo-induced electrons, which boost the reduction of Fe^{3+} to

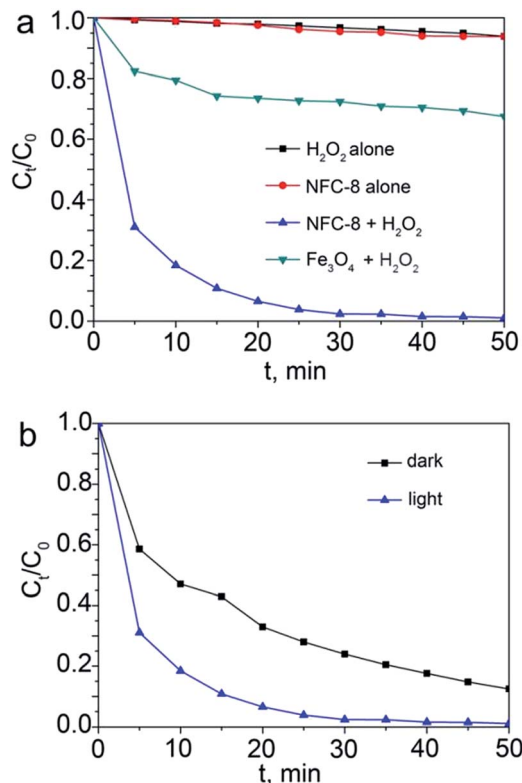Fig. 9 (a) Control tests for MB degradation with NFC-8 alone, H_2O_2 alone, NFC-8 with H_2O_2 together, and Fe_3O_4 with H_2O_2. (b) Degradation of MB with NFC-8 in dark and under irradiation.

Fe^{2+} again,[49,50] and thus improving the generation rate of hydroxyl radicals by ensuring supply of Fe^{2+} to react with H_2O_2. For comparing the degradation efficiency of various samples, we have added the compared curves between NFC-2, NFC-5, NFC-8 and NFC-12 in Fig. S9.† It can be seen NFC-8 shows the highest degradation efficiency. For NFC-2, the main products are Fe_4N and Fe_3C. With the amount of dicyandiamide increasing, the peaks of Fe_4N disappear and the peaks of Fe_3C become stronger and sharper in NFC-5 and NFC-8, which indicates that the phase of Fe_3C becomes the major component in the resulted products. From NFC-2 to NFC-8, the content of nitrogen in Fe–C system decreases, however the degradation efficiency increases. Whene structure of Fe_3C becomes the major component, NFC-8 shows the highest degradation efficiency. The doping of nitrogen enhances the catalytic activity of Fe_3C, however too much nitrogen atoms may destroy the structure of Fe_3C which can hinder the conduction of electron. For NFC-12, the intensity of diffraction peaks of Fe_3C and Fe_5C_2 drops, because of excessive carbon in structure. More amorphous carbon structure on the surface decreases the catalytic activity. For NFC-8, a certain amount of nitrogen increases the absorption of irradiation however not decrease the conduction of electron.

Conclusions

In summary, visible-light responsive NFC-8 as an efficient heterogeneous photo-assisted Fenton catalyst was successfully

prepared in this work. The nitrogen doped graphitic carbon layers enhanced the absorption of light and the defects on the surface reduce the recombination rate of photo-induced electron hole pairs. The iron bound with nitrogen doped graphitic carbon on surfaces functioned as catalytic active sites in photo-assisted Fenton process, and the catalytic activity greatly enhanced by introducing illumination. The experiment of degrading methylene blue demonstrated the excellent catalytic ability of NFC-8 particles under light even though it was used at neutral pH and the removal rate of methylene blue reached 95% in 20 minutes under the optimum condition of 0.75 g L^{-1} catalysts and 0.15 M H_2O_2. Overall, the results of NFC-8 particles as photo-assisted Fenton catalysts indicated that Fe_3C-based materials were potential Fenton-like catalysts in industrial applications.

Acknowledgements

Notes and references

1 Y. Z. Chen, N. Li, Y. Zhang and L. D. Zhang, *J. Colloid Interface Sci.*, 2014, **422**, 9.

2 M. L. Rache, A. R. García, H. R. Zea, A. M. T. Silva, L. M. Madeira and J. H. Ramírez, *Appl. Catal., B*, 2014, **146**, 192.

3 F. Yu, J. Ma and S. Han, *Sci. Rep.*, 2014, **4**, 5326.

4 J. Ponou, T. Ide, A. Suzuki, H. Tsuji, L. P. Wang, G. Dodbiba and T. Fujita, *Water Sci. Technol.*, 2014, **69**, 1249.

5 T. Matsui, S. Suzuki, Y. Katayama, K. Yamauchi, T. Okanishi, H. Muroyama and K. Eguchi, *Langmuir*, 2015, **31**, 11717.

6 X. J. Yang, X. M. Xu, J. Xu and Y. F. Han, *J. Am. Chem. Soc.*, 2013, **135**, 16058.

7 Z. J. Li, G. Ali, H. J. Kim, S. H. Yoo and S. O. Cho, *Nanoscale Res. Lett.*, 2014, **9**, 276.

8 P. Avetta, A. Pensato, M. Minella, M. Malandrino, V. Maurino, C. Minero, K. Hanna and D. Vione, *Environ. Sci. Technol.*, 2015, **49**, 1043.

9 S. Guo, Y. Zhu, Y. Yan, Y. Min, J. Fan and Q. Xu, *Appl. Catal., B*, 2016, **185**, 315.

10 Z. Ai, L. Lu, J. Li, L. Zhang, J. Qiu and M. Wu, *J. Phys. Chem. C*, 2007, **20**, 7430.

11 T. Han, L. Qu, Z. Luo, X. Wu and D. Zhang, *New J. Chem.*, 2014, **38**, 942.

12 M. A. De León, M. Sergio, J. Bussi, G. Ortiz de la Plata, A. E. Cassano and O. M. Alfano, *Ind. Eng. Chem. Res.*, 2015, **54**, 1228.

13 S. Guo, Y. Zhu, Y. Yan, Y. Min, J. Fan and Q. Xu, *J. Mater. Chem. A*, 2014, **2**, 2578.

14 S. Guo, Y. Zhu, Y. Yan, Y. Min, J. Fan and Q. Xu, *ACS Appl. Mater. Interfaces*, 2016, **8**, 2928.

15 Z. Xu, C. Huang, L. Wang, X. Pan, L. Qin, X. Guo and G. Zhang, *Ind. Eng. Chem. Res.*, 2015, **54**, 4593.

16 J. Herney-Ramirez, M. A. Vicente and L. M. Madeira, *Appl. Catal., B*, 2010, **98**, 10.

17 M. Wang, L. Sun, J. Cai, P. Huang, Y. Su and C. Lin, *J. Mater. Chem. A*, 2013, **11**, 2082.

18 F. Martínez, G. Calleja, J. A. Melero and R. Molina, *Appl. Catal., B*, 2005, **60**, 181.

19 M. Tekbaş, H. C. Yatmaz and N. Bektaş, *Microporous Mesoporous Mater.*, 2008, **115**, 594.

20 F. Martínez, G. Calleja, J. A. Melero and R. Molina, *Appl. Catal., B*, 2007, **70**, 452.

21 S. Guo and G. Zhang, *RSC Adv.*, 2016, **6**, 2537.

22 S. Rahim Pouran, A. A. Abdul Raman and W. M. A. Wan Daud, *J. Cleaner Prod.*, 2014, **64**, 24.

23 F. Velichkova, C. Julcour-Lebigue, B. Koumanova and H. Delmas, *J. Environ. Chem. Eng.*, 2013, **1**, 1214.

24 R. Sharma, S. Bansal and S. Singhal, *RSC Adv.*, 2015, **5**, 6006.

25 L. Vocadlo, J. Brodholt, D. P. Dobson, K. S. Knight, W. G. Marshallc, G. D. Pricea and I. G. Wooda, *Earth Planet. Sci. Lett.*, 2002, **203**, 567.

26 L. Zhang, H. B. Wu, S. Madhavi, H. H. Hng and X. W. Lou, *J. Am. Chem. Soc.*, 2012, **134**, 17388.

27 J. Liang, R. F. Zhou, X. M. Chen, Y. H. Tang and S. Z. Qiao, *Adv. Mater.*, 2014, **26**, 6074.

28 W. Li, H. Qi, X. Niu, F. Guo, X. Chen, L. Wang and B. Lv, *RSC Adv.*, 2016, **6**, 24820.

29 T. Wu, H. Zhang, X. Zhang, Y. Zhang, H. Zhao and G. Wang, *Phys. Chem. Chem. Phys.*, 2015, **17**, 27527.

30 Y. Hu, J. O. Jensen, W. Zhang, S. Martin, R. Chenitz, C. Pan, W. Xing, N. J. Bjerrum and Q. Li, *J. Mater. Chem. A*, 2015, **3**, 1752.

31 W. Yang, X. Yue, X. Liu, L. Chen, J. Jia and S. Guo, *Nanoscale*, 2016, **8**, 959.

32 Y. Hou, T. Huang, Z. Wen, S. Mao, S. Cui and J. Chen, *Adv. Energy Mater.*, 2014, **4**, 1400337.

33 X. Wang, K. Maeda, A. Thomas, K. Takanabe, G. Xin, J. M. Carlsson, K. Domen and M. Antonietti, *Nat. Mater.*, 2009, **8**, 76.

34 X. Yang, F. Qian, G. Zou, M. Li, J. Lu, Y. Li and M. Bao, *Appl. Catal., B*, 2016, **193**, 22.

35 Y. Zhu, J. Shen, K. Zhou, C. Chen, X. Yang and C. Li, *J. Phys. Chem. C*, 2011, **115**, 1614.

36 J. Shen, Y. Zhu, K. Zhou, X. Yang and C. Li, *J. Mater. Chem.*, 2012, **22**, 545.

37 B. K. Barman and K. K. Nanda, *Green Chem.*, 2016, **18**, 427.

38 X. Wang, P. Zhang, W. Wang, X. Lei and H. Yang, *RSC Adv.*, 2015, **5**, 57828.

39 X. B. Wang, P. Zhang, J. J. Gao, X. D. Chen and H. Yang, *Dyes Pigm.*, 2015, **112**, 305.

40 K. Dai, L. Lu, Q. Liu, G. Zhu, X. Wei, J. Bai, L. Xuan and H. Wang, *Dalton Trans.*, 2014, **43**, 6295.

41 H. Bi, W. Zhao, S. Sun, H. Cui, T. Lin, F. Huang, X. Xie and M. Jiang, *Carbon*, 2013, **61**, 116.

42 C. Han, Y. Wang, Y. Lei, B. Wang, N. Wu, Q. Shi and Q. Li, *Nano Res.*, 2014, **8**, 1199.

43 X. Du, H. Y. Liu and Y. W. Mai, *ACS Nano*, 2016, **10**, 453.

44 Y. Yao, Y. Cai, F. Lu, J. Qin, F. Wei, C. Xu and S. Wang, *Ind. Eng. Chem. Res.*, 2014, **53**, 17294.

45 E. P. Sajitha, V. Prasad, S. V. Subramanyam, A. K. Mishra, S. Sarkar and C. Bansal, *J. Phys.: Condens. Matter*, 2007, **19**, 046214.

46 Y. Kuang, Q. Wang, Z. Chen, M. Megharaj and R. Naidu, *J. Colloid Interface Sci.*, 2013, **410**, 67.

47 E. G. Garrido-Ramírez, B. K. G. Theng and M. L. Mora, *Appl. Clay Sci.*, 2010, **47**, 182.

48 H. Bel Hadjltaief, P. Da Costa, M. E. Galvez and M. Ben Zina, *Ind. Eng. Chem. Res.*, 2013, **52**, 16656.

49 X. Yang, W. Chen, J. Huang, Y. Zhou, Y. Zhu and C. Li, *Sci. Rep.*, 2015, **5**, 10632.

50 L. Liu, W. Yang, Q. Li, S. Gao and J. K. Shang, *ACS Appl. Mater. Interfaces*, 2014, **6**, 5629.